

Scalable Surrogate Verification of Image-based Neural Network Control Systems using Composition and Unrolling

Feiyang Cai^{1,3}, Chuchu Fan², and Stanley Bak¹

¹Department of Computer Science, Stony Brook University

²Department of Aeronautics and Astronautics, MIT

³School of Computing, Clemson University

E-mails: *feiyang@clemson.edu, chuchu@mit.edu, and stanley.bak@stonybrook.edu*

Abstract—Verifying safety of neural network control systems that use images as input is a difficult problem because, from a given system state, there is no known way to mathematically model what images are possible in the real-world. We build upon recent work that considers a surrogate verification approach, training a conditional generative adversarial network (cGAN) to use as an image generator in place of the real world. This setup enables set-based formal analysis of the closed-loop system, providing analysis beyond simulation and testing.

While existing work is effective on small examples, excessive overapproximation both within a single control period (one-step error) and across multiple control periods (multi-step error) limits its scalability. We propose approaches to overcome these two sources of error. First, we overcome one-step error by composing the system’s dynamics along with the cGAN and neural network controller, without losing the dependencies between input states and the control outputs as in the monotonic analysis of the system dynamics. Second, we reduce multi-step error by repeating the single-step composition, essentially unrolling multiple steps of the control loop into a large neural network. We then leverage existing network verification algorithms to compute accurate reachable sets for multiple steps, avoiding the accumulation of abstraction error at each step.

We demonstrate the effectiveness of our approach in terms of both accuracy and scalability using two case studies: an autonomous aircraft taxiing system based on Boeing’s TaxiNet and an advanced emergency braking system running within the CARLA simulator. On the aircraft taxiing system, the converged reachable set is 175% larger using the prior baseline method compared with our proposed approach. On the emergency braking system, with 24x the number of image output variables from the cGAN, the baseline method fails to prove any states are safe, whereas our improvements enable set-based safety analysis.

Index Terms—neural network control system, conditional generative adversarial networks, reachability analysis

I. INTRODUCTION

Neural networks are key enablers of image-based control systems, where applications span from autonomous vehicles [1] to industrial robotics [2]. Unfortunately, neural networks rarely come with guarantees of robustness or worst-case behaviors due to the inherent non-zero error rates and are often susceptible to low-noise adversarial attacks [3], [4].

In safety-critical scenarios, ensuring the safety and reliability of neural network control systems (NNCS) is paramount. The deployment of such systems demands rigorous *closed-loop* verification to show that hazardous situations are avoided. Although considerable strides have been made in verifying NNCS [5]–[7], the verification of *image-based* NNCS is underexplored. Image-based NNCS verification is more difficult—the image observation is a high dimensional input and vision networks are typically more complex than control networks, employing convolutional or transformer layers. Scalability aside, such verification problems are even hard to formulate, since reasoning over the set of images possible in the real world is not a precise mathematical statement.

One approach around this problem involves using generative models to replace the real-world perception system, paving the way for the formal verification of image-based NNCS [8]. This technique first trains a conditional generative adversarial network (cGAN) [9] to approximate the perception system, generating images based on the system states. The concatenation of cGAN and controller results in a unified neural network controller with low-dimensional state inputs. This surrogate controller allows existing verification approaches [10], [11], which combine neural network verification tools and reachability analysis, to be applied.

However, the previous verification methodology [8] suffers from being overly conservative, computing the reachable sets with significant overapproximation. There are two main sources of overapproximation, *one-step error* and *multi-step error*. Within a single control period, the prior work computes the intervals of the control outputs and then applies monotonic analysis of the system dynamics to obtain the reachable sets, without considering the dependencies between the input states and control outputs, causing one-step error. Additionally, discrete abstraction of reachable sets after each step introduces multi-step error. The interaction of these two sources of error produces considerable overapproximation, potentially leading to false positives. As image-based NNCS grow in complexity and incorporate modern neural network architectures, extending the verification techniques to encompass these complexities presents additional challenges.

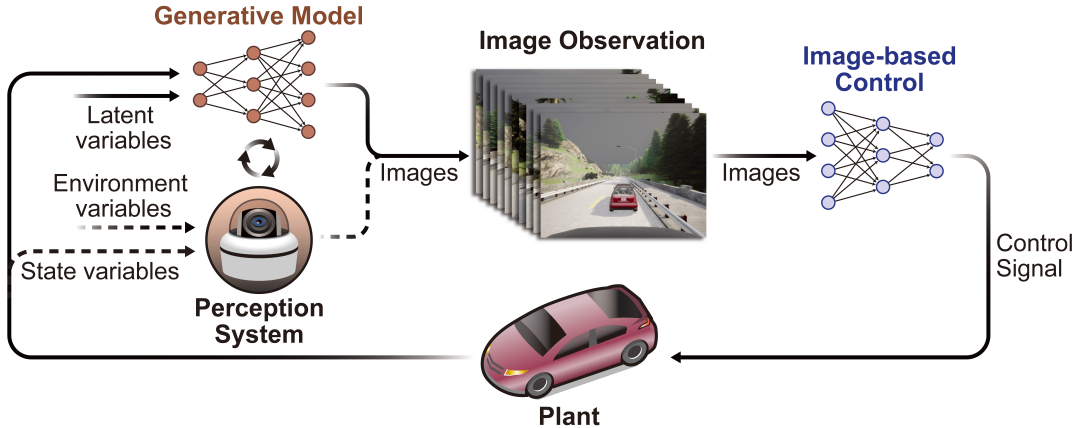


Fig. 1: Simplified architecture of an image-based neural network control system and its surrogate system.

This work builds upon the surrogate verification approach using cGAN and focuses on mitigating overapproximation within the existing method. The first improvement is to compose the discrete-time dynamics along with the cGAN and neural network controller. This composition preserves the dependencies between the states and control signals, reducing one-step error. We introduce two distinct composition options to accommodate varying network scales and system dynamics. One option involves incorporating the dynamics as an additional layer within the networks, allowing direct handling by neural network verification tools. This approach may encounter challenges when nonlinear dynamics are not supported by these tools or when overapproximation of nonlinear functions in the dynamics causes infinite outputs. The other composition option combines neural network exact analysis [12] with the reachability algorithms from hybrid systems [13]. This method computes more accurate reachable sets using the star set representation [14], further reducing the one-step error. This approach is applicable when the network’s scale is moderate and the network exclusively employs ReLU activation functions. Instead of limiting the verification scope to a single step, we propose another improvement by unrolling multiple steps of the control loop into a unified, larger neural network. We then leverage state-of-the-art network verification tools, specifically α - β -CROWN [15] and nnum [12], to compute reachable sets over multiple steps. This unrolling strategy reduces the frequency of abstraction operations and, consequently, minimizes the multi-step error.

We evaluate our method with two case studies. The first focuses on an autonomous aircraft taxiing system [8] based on Boeing’s TaxiNet [16], featuring a feed-forward neural network controller. The evaluation demonstrates that the proposed approach significantly reduces overapproximation, and the reachable set upon convergence using the prior baseline method is 175% larger than with our proposed approach. Therefore, our method can verify scenarios where the existing approach fails. The second case is an advanced emergency braking system [17] within the CARLA simulator [18], incorporating modern image-based controllers in the loop. This work stands as the first attempt to conduct reachability analysis

for a closed-loop system with convolutional and transformer layers.

II. BACKGROUND

In this section, we begin by presenting the system model and formulate the verification problem for the image-based NNCS. Subsequently, we introduce the surrogate approximation of the perception system using the generative models and elucidate the fundamental rationale behind this approach. Finally, we discuss the challenges in verifying such a surrogate system and limitations of existing methods.

A. Problem Formulation

Definition 1 (System Model): Consider an autonomous system with an image-based neural network controller, as depicted in Fig. 1. We assume that, at step k , the ego system is in a state $x_k \in \mathcal{X}$. The *perception system* P , employs a camera sensor to observe the surrounding environment, characterized by $e_k \in \mathcal{E}$, and translates these observations into a representative image $o_k \in \mathcal{O}$. Following this, the image o_k is input into an *image-based controller* C to generate a control command $u_k \in \mathcal{U}$ to accomplish a specific task¹. Driven by the control command u_k , the system’s state transitions from the current state x_k to a subsequent state x_{k+1} in accordance with the discrete *dynamics* D , thereby closing the loop of the system operation. The evolution of the system over a single step depends on both the current state x_k and the environment status e_k , and can be expressed as:

$$x_{k+1} = D(x_k, C(P(x_k, e_k))). \quad (1)$$

Definition 2 (System Evolution): The system starts from an initial state x_0 within a set $\mathcal{I} \subseteq \mathcal{X}$. At each time step i between 0 and $k-1$, the corresponding environment is represented as e_i , where $e_i \subseteq \mathcal{E}$. Consequently, the system state x_k evolves from x_0 by unrolling the dynamics defined in Eq. (1). This system evolution depends on the initial state x_0 and the series of the environment parameters $e_0, \dots, e_i, \dots, e_{k-1}$ over time:

$$x_k = \text{System}(x_0, \{e_0, \dots, e_i, \dots, e_{k-1}\}). \quad (2)$$

¹The inputs to the controller may encompass additional sensor measurements based on the system state, which have been omitted in the paper.

Definition 3 (Reachable Set): According to Definition 2, the reachable set at time step k is:

$$R_k = \{\text{System}(x_0, \{e_0, \dots, e_{k-1}\}) \mid \forall x_0 \in \mathcal{I}, \forall_{i \in [0, k-1]} e_i \in \mathcal{E}\}.$$

Here, R_0 denotes the reachable set at time step 0, which is equal to the initial set \mathcal{I} . Furthermore, the reachable set over the time interval $[0, k]$ is defined as:

$$R_{[0, k]} = \bigcup_{i \in [0, k]} R_i.$$

Problem 1 (Safety Verification for Image-Based NNCS): The objective of the safety verification for image-based NNCS is to check whether the computed reachable set adheres to the system’s safety property. Formally, given an unsafe region $\mathcal{U} \subseteq \mathcal{X}$, the safety of the NNCS within a bounded time step k_{\max} can be verified if and only if the following condition is satisfied:

$$R_{[0, k_{\max}]} \cap \mathcal{U} = \emptyset.$$

B. Perception System Approximation using Generative Models

One of the most significant challenges in verifying image-based control systems is formalization of the perception system. Consider a camera used for autonomous driving. For instance, one might attempt to verify a specification that involves a neural network and states, “all images with a car that is 5 meters ahead are predicted as such.” However, such a specification becomes difficult to formalize due to the interdependence of the captured images on multiple factors. As illustrated in images in Fig. 1, these factors include both the system state x , such as the distance between the ego car and the leading car, and the environment e , such as the appearance of the leading car, weather conditions, road lane count, and the presence of other objects on the road or sidewalks². The challenge lies in providing a clear mathematical and comprehensive description for such a specification.

Rather than considering “all images with a car that is 5 meters ahead,” we could instead first train a neural network to provide us the distance of a car in a given image, and then consider the more precisely defined set of “all images with a car that is *predicted* to be 5 meters ahead.” However, this property could become a tautology if the same network is used in the specification and in the analysis, leading to a specification like “all images with a car predicted 5 meters ahead are predicted to be a car 5 meters ahead.” Even if a different network is used, such specifications become challenging to verify due to the need for global quantification across all images.

An alternative approach has recently been proposed [8] where, images generated by a conditional generative adversarial network (cGAN) [9] are used to replace the images rendered by the actual perception system for the purpose of verifying the image-based NNCS. In this context, the specification can be formalized as “all images that can be produced by a specific cGAN are predicted to be a car 5 meters ahead.” Such a specification is practical to work with, and in this paper, we embrace this methodology to establish

²The generated images are also affected by physical parameters of the camera, and it is simply omitted in the paper.

the verification problem for the closed-loop system. Of course, safety of the cGAN does not guarantee safety in the real world, but this approach does offer an analysis method for this class of systems beyond just running simulations and tests.

The cGAN learns the distribution of images conditioning on some auxiliary information and can be used to approximate the original perception system \mathbb{P} into a *surrogate perception system* denoted as $\hat{\mathbb{P}}$. The generator of the cGAN maps the conditional information c and a set of latent variables z into an image observation \hat{o} . When the cGAN serves as a perception surrogate, the conditional information c corresponds to the system states x , guiding the generator to create images relevant to the desired information. It is worth noting that controlled environmental settings could also be encoded in the conditions, although we omit this aspect in the present paper, leaving it as a potential avenue for future exploration. Given the multitude of environmental variables influencing image generation, explicitly encoding and controlling all of them is practically infeasible. Hence, the environmental variables e are left uncontrolled and represented by latent variables z within the cGAN.

Definition 4 (Surrogate System Model): The one-step system evolution with the surrogate perception system is defined as:

$$x_{k+1} = D(x_k, C(\hat{\mathbb{P}}(x_k, e_k))).$$

Problem 2 (Surrogate Verification for Image-Based NNCS): Instead of verifying the actual system as defined in Problem 1, this paper focuses on the verification of the surrogate system.

C. Verification Challenges

The concatenation of the cGAN and the image-based controller into a unified neural network transforms the entire system into a state-based NNCS. In this way, the image-based NNCS can be analyzed using existing methodologies designed for verifying state-based NNCS [10], [11]. However, computing reachable sets for an NNCS can still be challenging [11]. In this case, the problem is exacerbated because the neural network is very complex, performing both image generation and image processing tasks. In contrast, in the most recent NNCS verification competition, ARCH-COMP 2023 [19], the analyzed neural networks generally had only a few dozen neurons and up to 6 layers. Most conventional NNCS verification tools [20], [21], including those that participated the competition, lack support for convolutional neural networks. Even among those that do offer support [6], encountering large-scale networks leads to significant overapproximations at each step. These overapproximations accumulate and expand, ultimately causing the tool to fail.

In the earlier work [8], to practically address the verification of the surrogate image-based control system, input images are downsized to small grayscale images, and the cGAN and image-based controller are implemented using medium-size feed-forward neural networks. Still, this method exhibits large overapproximation of the reachable sets. Such substantial overapproximation could result in instances where the overapproximated reachable sets intersect with unsafe regions, leading to the failure of safety verification. Moreover, as the input

images and network architectures of contemporary image-based control systems grow in complexity, employing high-resolution images rich in information and intricate network architectures like convolutional and transformer layers, the task of verification becomes even more challenging. **The main contribution of this paper is to address these challenges and reduce the overapproximation error.**

III. METHODOLOGY

In this section, we start to analyze the underlying causes of the overapproximation within the prior method [8]. Following this, we present the proposed method designed to mitigate the overapproximation and improve the verification performance for the surrogate image-based NNCS.

A. Overapproximation Analysis

Consider Problem 2, where a surrogate image-based NNCS starts from an initial set R_0 . The verification task is to determine whether the reachable set up to time k_{\max} satisfies the safety property, i.e, avoiding any intersection with the unsafe set \mathcal{U} . Neural network verification tools are commonly employed to prove properties over the input and output of the network. Therefore, if the system's evolution function, as defined by Eq. (2), can be combined into a unified neural network NN, the closed-loop system property can be verified using neural network verification tools. Formally, the set of possible outputs of the network (system state at step k_{\max}) is:

$$\begin{aligned} \text{Range}(\text{NN}, R_0, \mathcal{E}^{k_{\max}}) = & \{\text{NN}(x_0, \{e_0, \dots, e_{k_{\max}-1}\}), \\ & | \forall x_0 \in R_0, \forall i \in [0, k_{\max}-1] e_i \in \mathcal{E}\}. \end{aligned}$$

The neural network verification problem is to check if $\text{Range}(\text{NN}, R_0, \mathcal{E}^{k_{\max}}) \cap \mathcal{U} = \emptyset$. However, such a verification task presents several challenges. Firstly, the system dynamics often involve nonlinear operations that may not be supported by verification tools. Secondly, these tools may have scalability limitations in that large input sets and complex neural networks may present intractable verification problems. Unrolling the system evolution function to span from time step 0 to k_{\max} replicates a sequence of cGANs, image-based controllers, and dynamics layers. This composed network can be too complex even for state-of-the-art neural network verification tools.

To address these challenges, a practical approach integrating neural network verification tools with reachability methods was proposed in previous works [10], [11], later extended to verify the surrogate image-based NNCS [8]. This method serves as a baseline for comparison in this paper.

To make the problem tractable, the prior approach constructs and analyzes a discrete existential abstraction of the system, with transitions defined using one-step reachability. The process starts by dividing the state space into a finite number of rectangular cells along a grid, denoted as \mathcal{H} . The initial states in R_0 are then abstracted using a set of rectangular cells referred to as \mathcal{C}_0 , where $R_0 \subseteq \mathcal{C}_0 \subseteq \mathcal{H}$. For each cell c within \mathcal{C}_0 , the interval bounds on the control commands are determined using a neural network verification tool. These bounds are combined with a monotonic analysis of the system dynamics to result in an interval of possible

one-step successors from state cell c , called \mathcal{R}_1^c . For example, in the autonomous aircraft taxiing system case study we will analyze later, the dynamics updating function for the heading angle error θ is: $\theta_{k+1} = \theta_k + \frac{v}{L} \Delta t \tan \phi_k$, where v , L and Δt are constants, ϕ_k is the control signal, steering angle of the aircraft. As the tan function is monotonically increasing in the specified operating region, monotonic analysis computes the upper (lower) bound of θ_{k+1} by simultaneously substituting the upper (lower) bounds for both θ_k and ϕ_k into the dynamics updating function [8].

The set of possible successor states from c is then the set of cells \mathcal{C}_1^c that overlap with \mathcal{R}_1^c . An overapproximation of the reachable set for the entire initial state is then the union of all successors from individual cells, $\mathcal{C}_1 = \bigcup_{c \in \mathcal{C}_0} \mathcal{C}_1^c$, which overapproximates the set $\mathcal{R}_1 = \bigcup_{c \in \mathcal{C}_0} \mathcal{R}_1^c$, and also the exact reachable set R_1 , denoted as $R_1 \subseteq \mathcal{R}_1 \subseteq \mathcal{C}_1$. This process is repeated iteratively to obtain reachable set \mathcal{C}_k for arbitrary time step k . The first row of Fig. 2 visually illustrates the computation flow from R_0 to \mathcal{C}_1 using this method, and the first row of Fig. 3 displays the resulting reachable sets from R_0 to \mathcal{C}_2 . Note that the latent space representing the environment is not divided, and thus, the entire set \mathcal{E} is considered by the verification tools when analyzing each cell.

However, this baseline method introduces considerable overapproximation error, which we call *one-step error* and *multi-step error*. The one-step error reflects the discrepancy between the overapproximated reachable set \mathcal{R} and the exact reachable set R within a single step. This type of error arises from two factors within the baseline method. First, the method computes the interval of the control outputs without accounting for the dependencies between the input states and control outputs; second, the method uses monotonic analysis for system dynamics, resulting in an interval enclosure of the reachable set for the next state, which is a coarse overapproximation of the exact reachable set. The one-step error is illustrated in the middle of the first row in Fig. 3, where, at step 1, the exact reachable set is a gray curvilinear triangle, while the baseline algorithm overapproximates it as a pink rectangle. The multi-step error, on the other hand, arises from the abstraction error when transitioning from \mathcal{R} to \mathcal{C} . As shown in the top middle in Fig. 3, after overapproximating the reachable set with the pink rectangle, the baseline method further abstracts it with 4 blue boxes, introducing the multi-step error.

As steps increase, both of these errors interact and accumulate, compromising the verification accuracy. At time step 2 in the top right in Fig. 3, with the baseline method, all 9 cells in the graph are considered reachable, while the exact reachable set occupies a curvilinear triangle smaller than 3 cells.

B. Proposed Improvements

In order to overcome the presented sources of error for the baseline method, we propose to use *composition* and *unrolling*.

1) *Composition*: One factor contributing to the one-step error is the neglect of dependencies between input states and control outputs. Composing the system dynamics along with the cGAN and controller within a single control period can preserve the dependencies, thereby reducing the one-step error. This computation flow is depicted in the second row of Fig. 2.

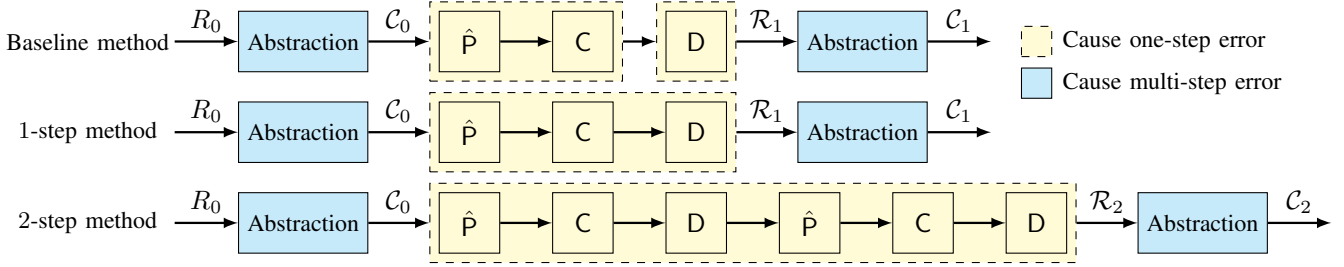


Fig. 2: Computation flowcharts for the baseline, 1-step, and 2-step methods, where \hat{P} , C , and D denote the surrogate perception system, image-based controller, and dynamics, respectively.

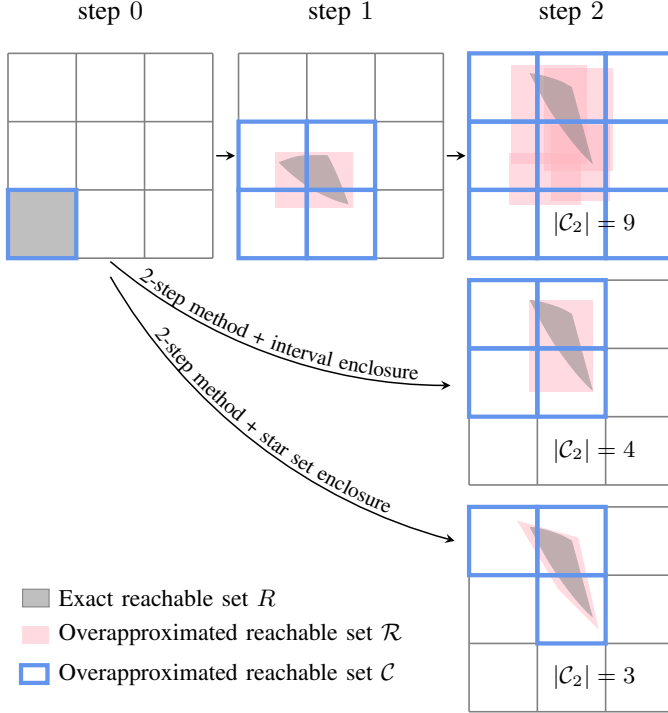


Fig. 3: Illustrations of reachable sets by using three different methods. The first row is the baseline method; the second row is the method employing the 2-step unrolling coupled with the composition approach wherein the dynamics is integrated as a layer of the networks; the third row is the method employing the 2-step unrolling coupled with the composition approach based on exact neural network analysis and reachability analysis. In this illustrative example, assume the initial exact reachable set R_0 only contains one cell c , $R_0 = \mathcal{C}_0 = \{c\}$.

The first proposed method for composition is to directly append the system dynamics to the neural networks as an additional layer. Verification tools can then assess the output specifications of a complete step given the input sets, internally preserving the dependencies between state and control. Rather than computing interval bounds on the control outputs, the tools would be used to compute interval bounds on the successor states. However, there are drawbacks to this composition method. First, this method assumes that the system dynamics are either linear or consist only of nonlinear

operations supported by a neural network verification tool. Even if the dynamics are supported, verification tools may still fail to produce bounds. For instance, many state-of-the-art neural network verification tools, like α, β -CROWN [15], are based on bounds propagation and refinement. Nonlinear functions like \tan , while supported, might have infinite outputs when their ranges are overapproximated—if the input to \tan is initially overapproximated as beyond $(-\frac{\pi}{2}, \frac{\pi}{2})$. In addition, although this composition method can result in a tighter interval enclosure of the reachable set compared to the baseline method, it is still not exact and can cause some one-step error.

A second alternative approach to composition involves combining dependency-preserving exact neural network analysis methods with reachability analysis algorithms from hybrid systems. Unlike bounds propagation methods (such as those used in α, β -CROWN), dependency-preserving methods such as those used in nenum [12] or NNV [6] provide the set of possible outputs along with their relationship to inputs, represented as a union of star sets [14] (sometimes called constrained zonotopes [22]). When dynamics are nonlinear, we use reachability analysis algorithms from hybrid systems, specifically the conservative linearization approach [13]. This method soundly overapproximates nonlinear systems as locally linear with added noise to account for the maximum linearization error. While this approach introduces some overapproximation from the linearization error, the reachable set is significantly more accurate than the monotonic analysis approach in the prior work, reducing one-step error. Additionally, this composition method does not have the infinite output problem when the dynamics involve \tan or other reciprocal functions. This composition method does have scalability limitations related to the size and type of the neural network, as exact analysis of the network is required.

2) *Unrolling*: Multi-step error is attributed to the abstraction operation from reachable set \mathcal{R} to a set of cells \mathcal{C} at each step. To reduce the frequency of abstraction operations and, consequently, the multi-step error, we propose to unroll multiple control periods and combine them into a single large neural network. This strategy composes multiple steps of analysis into a single larger operation, in order to avoid error caused by repeated application of the abstraction step. The third row of Fig. 2 illustrates this strategy with a 2-step unrolling. Increasing the number of unrolling steps m generally leads to a smaller overapproximation error, but a more complex verification problem at each step. Thus, the

selection of m depends on both the system complexity and the verification tool used.

3) *Improvement Illustration:* The composition and unrolling strategies collectively contribute to reducing overapproximation, as illustrated in the second and third rows of Fig. 3. The second row shows the method employing a 2-step unrolling strategy, coupled with the first composition approach wherein the dynamics are integrated as a layer within neural networks. This approach enables direct computation of the interval enclosure for reachable set at step 2, which is then abstracted into 4 cells, as opposed to the 9 cells in the baseline method shown in the first row. In the third row, we illustrate the method with a 2-step unrolling strategy, while using the composition based on exact neural network analysis and reachability algorithm for the system dynamics. The reachable set at step 2 is represented by star sets, which aligns more closely with the exact reachable set. By checking the intersection between the star sets and rectangular cells [23], the reachable set at time step 2 can be reduced to 3 cells compared to 4 cells using the interval enclosure.

4) *Overall Algorithm:* The pseudocode for the overall approach is presented in Algorithm 1. We start by initializing the global reachable set \mathcal{C} with a set of cells \mathcal{C}_0 abstracted from the initial set R_0 (line 2). The abstraction process is formally expressed as $\mathcal{C} = \alpha(\mathcal{R}, \mathcal{H})$, where \mathcal{H} is the set of all rectangular cells in the state space. Assuming the number of unrolling steps as m , we denote the computation of the reachable set after m steps \mathcal{R}_{k+m} from time step k as $\mathcal{R}_{k+m} = \text{ComputeReach}_m(\mathcal{C}_k)$. It should note that the computation process must be applied for each cell contained within \mathcal{C}_k , with the results then being combined to obtain the reachable set. However, using the operator ComputeReach_m alone allows us to compute reachable sets only when the time steps are multiples of m . To ensure soundness we must span the entire time domain, requiring ComputeReach_1 , ComputeReach_2 , up to $\text{ComputeReach}_{m-1}$.

Starting from \mathcal{C}_0 , we compute reachable sets \mathcal{R}_1 through \mathcal{R}_m , which are then abstracted into \mathcal{C}_1 to \mathcal{C}_m . These newly computed sets are accumulated into the global reachable set \mathcal{C} (line 6-10). The reachable set \mathcal{C}_m is used as the starting set for the next iteration (line 12). As \mathcal{C}_m serves an overapproximation of the exact reachable set R_m , computing the successor reachable sets from \mathcal{C}_m ensures the soundness of the reachability analysis. The iterative process continues until either the reachable set has converged to an invariant set, or the time step reaches the bounded step k_{\max} . Finally, the algorithm returns the global reachable set \mathcal{C} and a safety flag indicating if \mathcal{U} was reached.

5) *Backward Reachability Algorithm:* We additionally introduce a backward reachability algorithm designed to identify all cells within the state space that can be guaranteed to be safe. This algorithm is comprehensively outlined in Algorithm 2. This algorithm utilizes the backward reachability analysis to determine a set of cells \mathcal{A} within the state space that may potentially lead to unsafe system states, and the set of cells that can be guaranteed to be safe is essentially the complement of set \mathcal{A} . To streamline the process, the function of computing the reachable set (ComputeReach)

Algorithm 1: Proposed reachability algorithm.

```

1 Function ReachAnalysis ( $R_0, \mathcal{U}, m, k_{\max}, \alpha, \mathcal{H}$ ) :
   Input:  $R_0$ , initial set
   Input:  $\mathcal{U}$ , unsafe region
   Input:  $m$ , unrolling steps
   Input:  $k_{\max}$ , termination time step
   Input:  $\alpha$ , abstraction function
   Input:  $\mathcal{H}$ , rectangular cells defined within the state
       space
2    $\mathcal{C} := \mathcal{C}_0 := \alpha(R_0, \mathcal{H})$ 
3    $k := 0$ 
4    $isConverged := false$ 
5   while  $\neg isConverged$  and  $k < k_{\max}$  do
     /* compute reach set for  $k+1$  to  $k+m$  */
6     for  $i = 1$  to  $m$  do
7        $\mathcal{R}_{k+i} := \text{ComputeReach}_i(\mathcal{C}_k)$ 
8        $\mathcal{C}_{k+i} := \alpha(\mathcal{R}_{k+i}, \mathcal{H})$ 
9        $\mathcal{C} := \mathcal{C} \cup \mathcal{C}_{k+i}$ 
10    end
11     $isConverged := (\mathcal{C}_k = \mathcal{C}_{k+m})? true : false$ 
12     $k := k + m$ 
13  end
14   $isSafe := (\mathcal{C} \cap \mathcal{U} = \emptyset)? false : true$ 
15  return  $\mathcal{C}, isSafe$ 

```

and the abstraction process (α) can be combined into a single function ComputeReachCells . This function calculates the forward reachable cells starting from a single cell or a set of cells. Given that the input space is discretized into a finite number of cells, evaluating the forward reachable cells for each individual cell enables the construction of a reverse mapping $\text{ComputeBackReachCells}$, which can identify all cells that can reach a target cell or a set of target cells.

The algorithm for backward reachability analysis begins by initializing the set of potentially unsafe cells \mathcal{A} . This is done by considering the cells themselves as unsafe (line 2) or identifying cells that can reach an unsafe state through propagation using any one of the methods ranging from 1-step to $(m-1)$ -step approaches (lines 3-10). For each cell c that is newly added to \mathcal{A} , the algorithm computes all cells that could reach c using an m -step backward reachability analysis. These newly identified cells are considered potentially unsafe and are added to the set \mathcal{A} . This iteration continues until no new cells are added to \mathcal{A} , and the algorithm returns the set of possible unsafe cells \mathcal{A} within the state space.

Completeness Justification: If a cell is unsafe, it must reach an unsafe region at some step k in the future. Consider $k/m = a$ and $t\%m = b$. This cell must be included in the set computed using the following procedure defined within the algorithm. This set is obtained by first finding the set of cells that can reach an unsafe state using a b -step method (initialization procedure in the algorithm) and then back-propagating this set a times using an m -step method (iteration procedure in the algorithm).

Convergent Justification: Since the state space is quantized into a finite number of cells, it is impossible to add new cells

Algorithm 2: Proposed backward reachability algorithm.

```

1 Function BackReachAnalysis( $\mathcal{U}$ ,  $m$ ,  $\mathcal{H}$ ):
   Input:  $\mathcal{U}$ , unsafe region
   Input:  $m$ , unrolling steps
   Input:  $\mathcal{H}$ , rectangular cells defined within the state
       space
   /* initialize the possible unsafe set */
2  $\mathcal{A} := \mathcal{U} \cap \mathcal{H}$ 
3 foreach  $c \in \mathcal{H}$  do
4   for  $i = 1$  to  $m - 1$  do
5      $\mathcal{C} := \text{ComputeReachCells}_i(c)$ 
6     if  $\mathcal{C} \cap \mathcal{U} \neq \emptyset$  then
7        $\mathcal{A} := \mathcal{A} \cup \{c\}$ 
8     end
9   end
10 end
   /* Compute all possible unsafe cells using
        $m$ -step backward reachability */
11  $\mathcal{N} := \mathcal{A}$ 
12 while  $\mathcal{N} \neq \emptyset$  do
13    $\mathcal{N}' := \emptyset$ 
14   foreach  $c \in \mathcal{N}$  do
15      $\mathcal{C} := \text{ComputeBackReachCells}_m(c)$ 
16      $\mathcal{N}' := \mathcal{N}' \cup \mathcal{C}$ 
17   end
18    $\mathcal{N} := \mathcal{A} \cap \mathcal{N}'$ 
19    $\mathcal{A} := \mathcal{A} \cup \mathcal{N}'$ 
20 end
21 return  $\mathcal{A}$ 

```

to the set \mathcal{A} infinitely.

IV. CASE STUDIES

Our evaluation consists of two case studies. In Section IV-A we use the proposed approach to analyze an autonomous aircraft taxiing system [8] that uses Boeing’s TaxiNet [16]. In Section IV-B, we analyze a more complex image-based control system for an advanced emergency braking system [17] in the CARLA simulator [18].

A. Autonomous Aircraft Taxiing System

The autonomous aircraft taxiing system was the evaluation system used by the baseline method [8], which we use to demonstrate our proposed improvements. The system controls the steering of aircraft moving at a constant speed on a taxiway, using images captured by a camera on the aircraft’s right wing [10].

1) *System Details:* The state of the aircraft is defined by its crosstrack position p and heading angle error θ relative to the taxiway center line. Driven by the control signal ϕ , these state variables evolve according to nonlinear discrete dynamics:

$$\begin{bmatrix} p_{k+1} \\ \theta_{k+1} \end{bmatrix} = f(p_k, \theta_k; \phi_k) = \begin{bmatrix} p_k + v\Delta t \sin \theta_k \\ \theta_k + \frac{v}{L}\Delta t \tan \phi_k \end{bmatrix},$$

where v , Δt , and L represent the aircraft’s taxi speed (5 m/s), the dynamics updating period (0.05 s), and the distance between front and back wheels (5 m), respectively. The control signal ϕ_k is generated by an image-based controller that runs at 1 Hz. This controller first uses a neural network to predict the state variables \hat{p}_k and $\hat{\theta}_k$, and then a proportional control strategy generates the actual control signal by $\phi_k = -0.74\hat{p}_k - 0.44\hat{\theta}_k$. The perception system is approximated using a cGAN, taking the aircraft’s crosstrack position p and heading angle error θ as conditions. Two latent variables ranging from -0.8 to 0.8 are introduced to capture environment variations.

In the prior work with the baseline method, several simplifications were made to make the verification of the surrogate system tractable. First, the input images, originally 200×360 color images, were downsampled to 8×16 grayscale images. Second, the cGAN was initially trained using a deep convolutional GAN (DCGAN), but was then replaced by a smaller feed-forward neural network that emulates the image generation process of the DCGAN, in order to simplify analysis by the neural network verification tool. Two pairs of real images and the generated images using the network are shown in Fig. 4. The unified network, which includes both the cGAN and the image-based controller, consists of 7 fully-connected layers with ReLU activation functions.

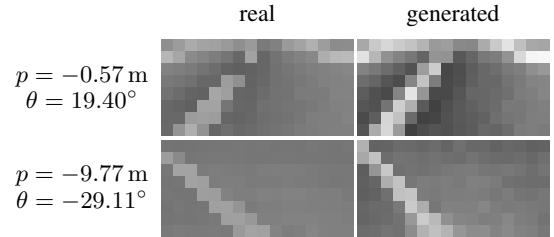


Fig. 4: Real images and generated images for the taxiing system, the case study considered by the baseline method.

2) *Verification Results:* The state space is defined with $p \in [-11 \text{ m}, 11 \text{ m}]$ and $\theta \in [-30^\circ, 30^\circ]$. Following the setting in prior work, we partition the space into a grid of 128×128 cells with uniform cell width in each dimension. The latent space z is not discretized. We initiate our comparison by contrasting the proposed method with the baseline approach through a single-cell reachability analysis. The proposed approach begins by composing the neural network and the system dynamics to preserve the dependencies between input states and control outputs. We first try to integrate the system dynamics as an additional layer within the neural networks. Despite the support for \sin and \tan within α, β -CROWN, the verification process *fails* in our experiment. This issue arises due to the infinite output of the \tan function during the initial refinement round, as discussed in Sec. III-B1.

We next try the proposed alternative composition approach, using exact analysis with nenum and reachability analysis. To account for the nonlinear dynamics, we employ a conservative linearization technique based on Taylor expansion [13]. This technique approximates the nonlinear dynamics with a 1st

order Taylor series and its 2nd order remainder:

$$x_{k+1}^i \in \overbrace{f^i(z_k^*) + \frac{\partial f^i(z)}{\partial z} \Big|_{z_k^*} (z_k - z_k^*)}^{1^{\text{st}} \text{ order Taylor expansion}} + L_i,$$

$A_{(i,\cdot)}$

where $x^T = [p, \theta]^T$ is the state vector, $z^T = [p, \theta, \phi]^T$ combines the states and input, and z^* is the expansion point, typically located at the center of the star set. Specifically, $A = \begin{bmatrix} 1 & v\Delta t \cos \theta & 0 \\ 0 & 1 & \frac{v}{L}\Delta t \tan^2 \phi \end{bmatrix}$, and the Lagrange remainders for the two state variables can be separately overapproximated using interval arithmetic [24] as:

$$L_1 \subseteq \frac{1}{2}v\Delta t[\min(-\sin \theta \cdot (\theta - \theta^*)^2), \max(-\sin \theta \cdot (\theta - \theta^*)^2)],$$

$$L_2 \subseteq \frac{v}{L}\Delta t[\min(\tan \phi \cdot (\tan^2 \phi + 1) \cdot (\phi - \phi^*)^2), \max(\tan \phi \cdot (\tan^2 \phi + 1) \cdot (\phi - \phi^*)^2)].$$

This reachability method tracks dependencies between the initial state and the next state under a control command, and therefore has less overapproximation error compared to monotonic analysis, as illustrated in Fig. 5. Starting from the same single cell (row 1, column 1), the pink reachable set in the proposed method (row 2, column 2), exhibits a smaller area compared to the pink box interval estimated by the baseline method (row 1, column 2). Furthermore, the number of abstract successor states is also reduced from 18 in the baseline method to 13 when dependency-preserving composition is used.

The multi-step unrolling strategy repeats the composition and propagates the resulting star sets across multiple steps. As illustrated in Fig. 5, the 2-step method (row 3, column 3) at step 2 significantly reduces overapproximation compared to the 1-step method (row 2, column 3), primarily by mitigating multi-step error. Consequently, when comparing the baseline method, 1-step method, and 2-step method at step 2, the number of reachable cells decreases from 55 to 40 to 25. Additionally, the reachable sets become closer to simulation results. As the number of steps m increases, the verification task become more complex to the growing scale of network architectures, and the expanding input dimensions with two additional latent variables at each step. In this experiment, we consider $m = 1, 2$.

Two properties are evaluated for the closed-loop system [8]:

- P1: The aircraft remains on the runway, ensuring that the magnitude of the crosstrack error does not exceed 10 m.
- P2: The aircraft is steered toward the runway center, leading to the convergence of the reachable set to an invariant set.

We begin by evaluating P2 using the same initial set as prior work [8], where $p \in [-10 \text{ m}, 10 \text{ m}]$ and $\theta \in [-10^\circ, 10^\circ]$. The simulations and reachable sets computed using the baseline, 1-step, and 2-step methods are depicted in the top row of Fig. 6. Over time, the reachable sets of all three methods gradually contract and eventually converge to invariant sets at 22 s, 22 s, and 26 s, respectively. This figure demonstrates P2, illustrating

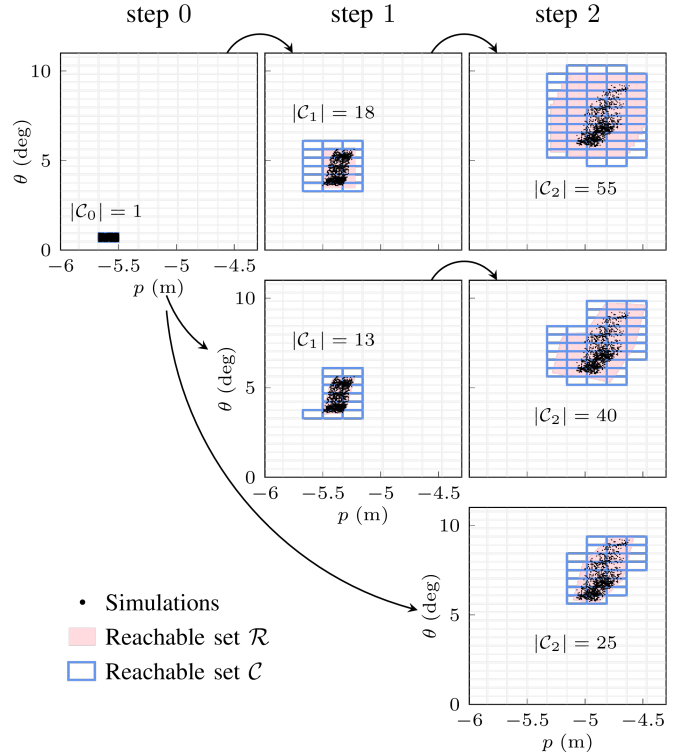


Fig. 5: Reachable sets computed using baseline method (first row), 1-step method (second row), and 2-step method (third row) in taxiing system. The initial set only contains one cell.

that the aircraft, guided by the image-based controller, converges to a position near the center of the runway. Further, the reachable sets computed using the baseline, 1-step, and 2-step methods progressively decrease and align more closely with the simulations. Upon convergence, the number of reachable cells for three methods are 661, 383, and 240, respectively. The steady state area with the baseline method is 175% larger than our two-step approach. These numerical results show that the proposed methods significantly reduce the overapproximation compared to the baseline method.

The importance of our accuracy improvements becomes more apparent when parameters of the case study are altered. To reduce verification time, we could consider a coarser grid with fewer cells. However, this results in more abstraction error. Another possible variant could consider a modified controller that converges more slowly. The convergence speed of the controller is important for verification, as it reduces the size of the reachable set and can compensate for overapproximation error in the analysis. We detail results on these variants in the bottom two rows of Fig. 6. In both scenarios, reachable sets computed by the baseline method extend beyond the taxiway, and P1 cannot be verified. The proposed methods effectively mitigate overapproximation, and successfully verify the safety of P1.

B. Advanced Emergency Braking System

We next evaluate the proposed approach using an advanced emergency braking system [17], [25] integrated with an image-

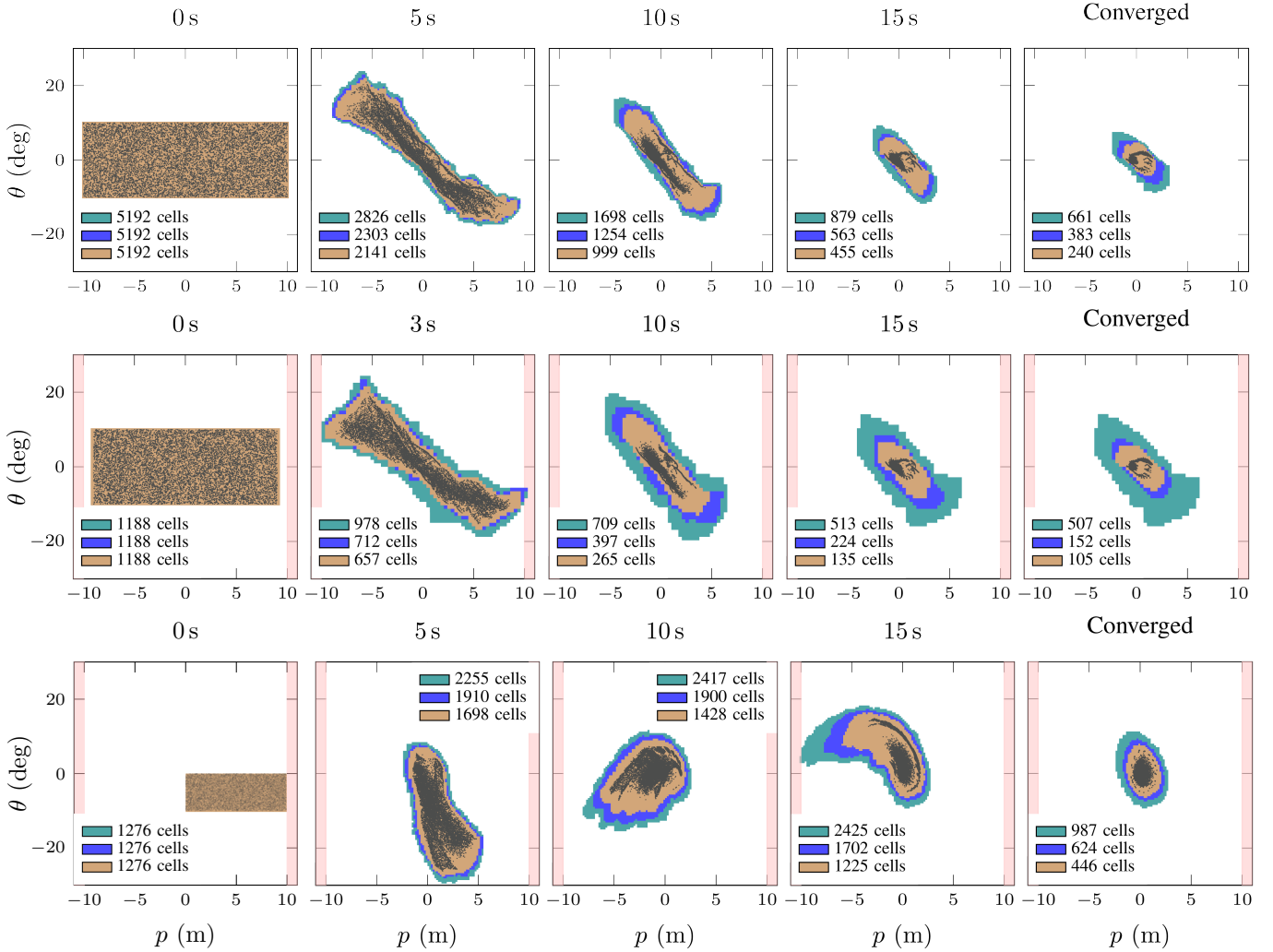


Fig. 6: Reachable sets over time using three different methods in the taxiing system. The colors black, teal, blue, and brown represent simulations, baseline, 1-step, and 2-step methods, respectively. The color pink denotes unsafe regions. Top: the experimental setting is same as the prior work [8], where the initial set is defined with $p \in [-10\text{ m}, 10\text{ m}]$ and $\theta \in [-10^\circ, 10^\circ]$; Middle: the height and width of the discretization cell are doubled, and the initial set is defined with $p \in [-9\text{ m}, 9\text{ m}]$ and $\theta \in [-10^\circ, 10^\circ]$. The baseline and 1-step methods fail to prove safety of the system at 3s, whereas 2-step method succeeds; Bottom: the image-based controller is trained with less episodes, and the initial set is defined with $p \in [0\text{ m}, 9.9\text{ m}]$ and $\theta \in [-10^\circ, 0^\circ]$. The baseline method fails to prove safety of the system at 15s, whereas 1-step and 2-step methods succeed.

based controller. The goal of this system is to apply braking force as needed to safely stop the host vehicle when approaching a stopped vehicle ahead. The purpose of this case study is to demonstrate that our improvements permit the verification of image-based NNCS that are significantly more complex than the prior work. In particular, the largest cGAN we consider produces 32×32 color images (Fig. 7), with 2300% more output variables than the 8×16 grayscale images in the aircraft taxiing system. Further, this result is the first, as far as the authors are aware, to verify properties of image-based NNCS that include more modern convolutional and transformer architectures, as opposed to only fully-connected layers with ReLU activation functions.

1) *System Details*: The system’s state is defined by the distance to the obstacle vehicle d , and the velocity of the host

vehicle v , and they evolve based on a linear discrete dynamics:

$$\begin{aligned} d_{k+1} &= d_k - v_k \Delta t, \\ v_{k+1} &= v_k - a_k \Delta t, \end{aligned}$$

where Δt is the time step (0.05 s). a_k is the deceleration of the host car, which is defined as $a_k = 0.009u_k + 0.0042$, where u_k is the braking force predicted by the image-based controller.

We consider two versions of an image-based controller: one implemented as a convolutional network, and the other as a transformer architecture. The perception system is abstracted using a cGAN, which incorporates the distance to the leading vehicle d as a conditional variable, along with four latent variables. In the analysis, we bound each of the latent variables by $\pm 10^{-2}$. The cGAN also comes in two network variants, each corresponding to a version of the controller network. The convolutional variant comprises a total of 8 convolutional lay-

ers, including both cGAN and controller, while the transformer variant includes a total of 22 convolutional layers and 2 self-attention layers. Detailed network architectures are available in Table I. Fig. 7 shows examples of real images and images generated by the two types of cGANs.

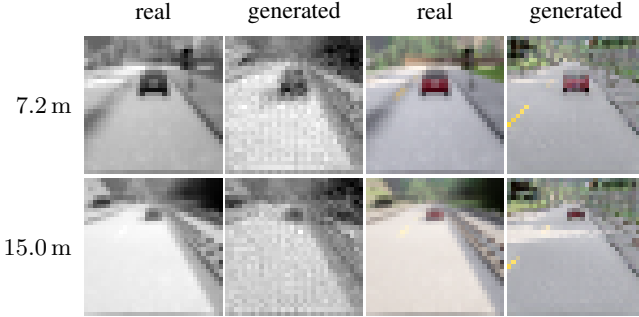


Fig. 7: Real images and generated images for the braking system. The grayscale images are from the convolutional network; the color images are from the transformer network.

TABLE I: Architectures of NNs in braking system; ResBlock and SelfAttention blocks refer to Self-Attention GAN [26].

(a) Generator (convolutional network)	
$z \in \mathbb{R}^4 \sim N(0, I); c \in \mathbb{R}$	
Concat(c, z) $\in \mathbb{R}^5$	
Dense $\rightarrow 2 \times 2 \times 128$, BN	
$(4 \times 4) \times 128$, stride = 2 ConvTranspose, BN, ReLU	
$(4 \times 4) \times 64$, stride = 2 ConvTranspose, BN, ReLU	
$(4 \times 4) \times 32$, stride = 2 ConvTranspose, BN, ReLU	
$(3 \times 3) \times 1$, stride = 1 ConvTranspose, Tanh	
(b) Controller (convolutional network)	
Grayscale image $\hat{o} \in \mathbb{R}^{32 \times 32 \times 1}$	
$(3 \times 3) \times 16$, stride = 2, padding = 1 Conv, ReLU	
$(3 \times 3) \times 32$, stride = 2, padding = 1 Conv, BN, ReLU	
$(3 \times 3) \times 64$, stride = 2, padding = 1 Conv, BN, ReLU	
$(3 \times 3) \times 128$, stride = 2, padding = 1 Conv, BN, ReLU	
Dense $\rightarrow 1$ ($\hat{d} \in \mathbb{R}^1$)	
Concat(\hat{d}, v) $\in \mathbb{R}^2$	
Dense $\rightarrow 400$, ReLU	
Dense $\rightarrow 300$, ReLU	
Dense $\rightarrow 1$, Clamp(0, 1)	

2) *Verification Results:* The state space with $d \in [0 \text{ m}, 60 \text{ m}]$ and $v \in [0 \text{ m/s}, 30 \text{ m/s}]$ is divided into a grid of 100×100 equal-size cells, while the latent space is not divided. Given the extensive scale and the non-ReLU activation functions in the network, performing composition with the exact analysis approach is infeasible. Instead, we perform composition the other way, by appending the linear dynamics to the neural networks as an additional layer and then running range analysis with α - β -CROWN. Since the state space is pre-divided, the process of abstracting reachable sets into cells can

(c) Generator (transformer network)	
$z \in \mathbb{R}^4 \sim N(0, I); c \in \mathbb{R}$	
Concat(c, z) $\sim \mathbb{R}^5$	
Dense $\rightarrow 4 \times 4 \times 256$	
ResBlock up, 256	
ResBlock up, 256	
SelfAttention, 256	
ResBlock up, 256	
BN, ReLU, $(3 \times 3) \times 3$, stride = 1 Conv, Tanh	

(d) Controller (transformer network)

RGB image $\hat{o} \in \mathbb{R}^{32 \times 32 \times 3}$	
ResBlock down, 128	
SelfAttention, 128	
ResBlock down, 128	
ResBlock, 128	
ResBlock, 256, ReLU	
Dense $\rightarrow 1$, Sigmoid, ($\hat{d} \in \mathbb{R}^1$)	
Concat(\hat{d}, v) $\in \mathbb{R}^2$	
Dense $\rightarrow 400$, ReLU	
Dense $\rightarrow 300$, ReLU	
Dense $\rightarrow 1$, Clamp(0, 1)	

be integrated into the verification process. For each output, we begin with simulations to determine the minimized range of the output, then identify the lower and upper indices of cells where all simulations are located. We incrementally expand the indices until the output is proved to be safe within the range. This approach allows us to effectively compute the reachable set represented by interval bounds.

For this system, we consider a single specification:

- P1: The host vehicle comes to a stop before colliding with the lead, meaning that the distance to the leading vehicle should never reach 0 m before the velocity reaches to 0 m/s.

First, we analyze the image-based controller using the convolutional network variant. We run 5000 simulations starting from random points in each cell, in order to estimate the number of possible safe cells. In Fig. 8a, 3463 cells within the state space are detected as unsafe using simulations, while the remaining cells are candidate safe cells. We unroll the system with $m = 1, 2$, and 3 steps, and run backward reachability analysis to show which states can be proven safe in Fig. 8a.

Surprisingly, no states can be proven safe using the 1-step method, even in situations with large distances and nearly-zero velocities. Compared with the aircraft taxiing system, the dynamics in this system moves the states significantly less at each control cycle, leading to excessive multi-step error from the abstraction process. This is illustrated in the first row of Fig. 9. Starting from cell (99, 0), the 1-step method extends the reachable set a cell located on the left, (98, 0) after one step. This trend continues, eventually extending reachable set to the leftmost cell where an unsafe state is reached. This experiment also demonstrates that the baseline method is ineffective in verifying such a system, given the 1-step method has lower overapproximation compared to the baseline

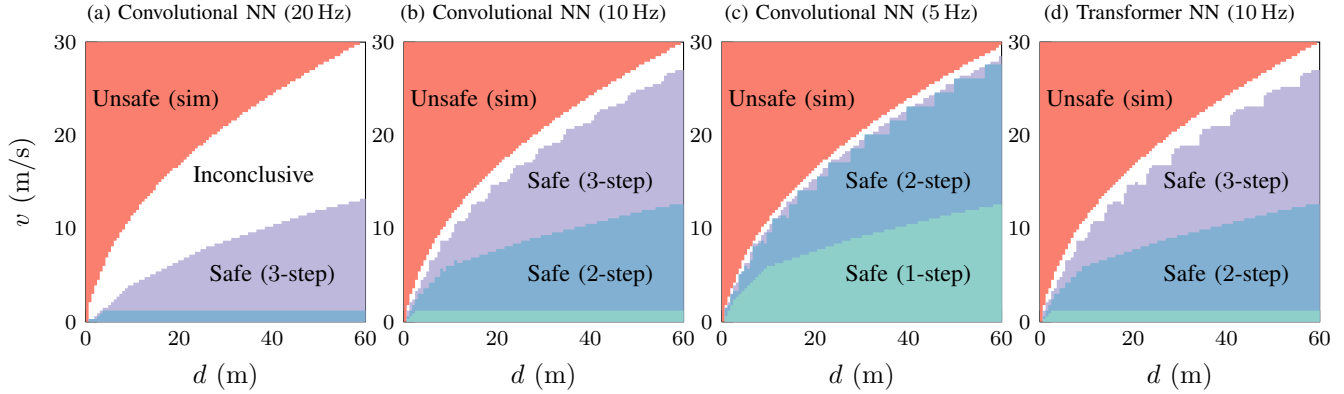


Fig. 8: The set of states guaranteed to satisfy the safety property within the state space for different controllers in the braking system. The controllers in (a), (b), and (c) are implemented using convolutional NN, differing in control periods, while the controller in (d) employs the transformer NN. Cells are identified as unsafe by the simulations are colored in red, with the corresponding counts of cells as 3463/3521/3617/3517 from left to right. The cells are verified as safe using 1-step, 2-step, and 3-step methods are colored in green, blue, and purple. For the 1-step method, the numbers of verified cells are 0/390/2859/390. For the 2-step method, these numbers are 384/2892/5883/2890, and for the 3-step method, they are 2669/5739/6035/5707.

approach. However, as shown in the second row, the 2-step method can prove the safety of cell (99, 0).

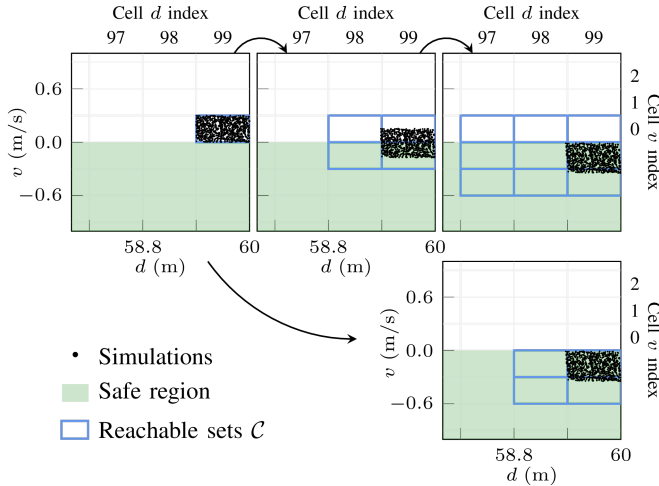


Fig. 9: Comparison of the reachable sets from a single cell computed by 1-step (first row) and 2-step methods (second row) in the braking system.

With the increase of unrolling steps m , the number of provably safe cells also increases. The 2-step and 3-step methods can verify the safety of 384 and 2669 cells, respectively. However, a substantial number of 3868 cells remain inconclusive. This occurs due to the control cycle’s period of 0.05 s, where even 3-step analysis has substantial multi-step error. Unrolling beyond 3 steps becomes practically difficult as the composed neural network increases in size, leading to an increase analysis time with the α - β -CROWN verification tool. Detailed results of runtime is provided in Table II. Verifying the system with the 1-step method requires approximately 125.14 GPU-hours (around 5 days). This time increases to 374.26 GPU-hours (around 15 days) for the 3-step method.

As the primary cause of inconclusive cells is multi-step

TABLE II: Verification times for all cells in the state graph. Note that these times are normalized to the times required by a single machine. These times are provided for reference, as experiments are conducted in parallel on multiple machines with different CPU and GPU configurations. The reported times are cumulative results across all machines.

	Taxiing system	Braking system	
		Convolutional	Transformer
1-step method	51.16 h	125.14 h	2630.88 h
2-step method	3954.77 h	168.67 h	3113.45 h
3-step method	N/A	374.26 h	3609.23 h

error from the abstraction process, we can consider decreasing the control frequency to reduce this effect. This is counterintuitive—a lower frequency should lead to *worse* control performance and therefore more unsafe cells. However, due to reduced multi-step error this could actually allow the method to verify more cells as provably safe.

We analyze the system by reducing the control frequency from 20 Hz to 10 Hz (Fig. 8b) and 5 Hz (Fig. 8c). As expected, the control performance becomes slightly worse as the control frequency decreases, resulting in a minor increase in the number of unsafe cells identified through simulation, by 1.7% for 10 Hz and 4.4% for 5 Hz. However, the decrease in control frequency improves the ability to establish provably safe cells for all methods compared to their original results—the white gap in the figure is reduced from 38.7% of the cells with the original 20 Hz frequency. For the 10 Hz controller, with 3-step analysis only 7.4% of the cells remain inconclusive. For the 5 Hz controller, this is further reduced to 3.5% of the cells.

We also evaluate the controller with transformer layers as shown in Fig. 8d, where simulations identify 3517 unsafe cells. As the m increases, the numbers of verified safe cells increase, reaching 390, 2890, and 5707 using 1-, 2-, and 3-step methods, respectively, while 7.8% of the cells remain inconclusive.

The usefulness of the surrogate verification is inherently tied to the quality, diversity, and fidelity of the images generated by cGANs. Despite extensive efforts to improve the visual quality and diversity of cGAN-generated images [27], [28], these images inevitably fall short in representing the entire actual observation space. Moreover, the intricate network architecture and numerous latent variables employed in modern cGANs challenges neural network verification tools, allowing only a subset of latent variables to be verifiable. Consequently, the verification becomes unnecessarily incomplete, potentially leading to false negatives. Existing strategies for enhancing diversity of the cGANs are primarily designed for categorical conditions and do not extend to the cGANs used in verifying image-based NNCS, where continuous system states serve as the condition labels. Although continuous conditional GANs (CcGANs) [29] have recently been introduced to adapt cGANs to continuous condition scenarios, it may compromise label consistency to improve visual diversity. Even without such trade-offs, our experiments indicate that cGANs can still produce images that slightly deviate from precise conditions. For example, a cGAN might generate images corresponding to “a car positioned 4.8 meters ahead” instead of the exact condition of “5 meters ahead.” Additionally, the process of generating images using cGANs does not consider the environmental context dependencies between consecutive image frames. If generated images from cGANs are concatenated into a sequence, each frame stands alone, and they cannot form a cohesive video. Both label inconsistency within a single frame and context inconsistency across multiple frames result in a loss of fidelity, potentially leading to false positives in verification.

VI. CONCLUSIONS

Analysis of image-based NNCS typically involves running lots of tests. By leveraging generative models to approximate the perception system, the surrogate verification approach offers a different avenue for analysis, which can leverage computational set-based analysis methods.

Scalability is the primary bottleneck in this line of work, and the main problem addressed in this paper. We have identified underlying causes of overapproximation error with the existing baseline method and proposed two strategies to overcome these problems based on composition and unrolling. In our evaluation, we have shown the benefits of our approach over the baseline method. In terms of accuracy, on the aircraft taxiing system the prior baseline method’s converged reachable set is 175% larger than with our approach. In terms of scalability, the transformer variant of the cGAN in emergency braking case study has over an order of magnitude (24x) more output pixels than the prior work’s case study.

Despite improvements, scalability is not yet solved, as state-of-the-art generative models complex and continue to grow in size. Increasing the ranges and number of latent variables, generating higher-resolution images, considering systems with more state variables and incorporating recent video GAN techniques [30] will all require further improvements to scalability.

- [1] C. Chen, A. Seff, A. Kornhauser, and J. Xiao, “Deepdriving: Learning affordance for direct perception in autonomous driving,” in *IEEE international conference on computer vision*, 2015.
- [2] S. Levine, P. Pastor, A. Krizhevsky, J. Ibarz, and D. Quillen, “Learning hand-eye coordination for robotic grasping with deep learning and large-scale data collection,” *International journal of robotics research*, 2018.
- [3] A. Bolor, K. Garimella, X. He, C. Gill, Y. Vorobeychik, and X. Zhang, “Attacking vision-based perception in end-to-end autonomous driving models,” *Journal of Systems Architecture*, 2020.
- [4] F. Cai, J. Li, and X. Koutsoukos, “Detecting adversarial examples in learning-enabled cyber-physical systems using variational autoencoder for regression,” in *IEEE Security and Privacy Workshops*, 2020.
- [5] X. Sun, H. Khedr, and Y. Shoukry, “Formal verification of neural network controlled autonomous systems,” in *ACM International Conference on Hybrid Systems: Computation and Control*, 2019.
- [6] H.-D. Tran, X. Yang, D. Manzananas Lopez, P. Musau, L. V. Nguyen, W. Xiang, S. Bak, and T. T. Johnson, “Nnv: the neural network verification tool for deep neural networks and learning-enabled cyber-physical systems,” in *International Conference on Computer Aided Verification*, 2020.
- [7] R. Ivanov, T. Carpenter, J. Weimer, R. Alur, G. Pappas, and I. Lee, “Verisig 2.0: Verification of neural network controllers using taylor model preconditioning,” in *International Conference on Computer Aided Verification*, 2021.
- [8] S. M. Katz, A. L. Corso, C. A. Strong, and M. J. Kochenderfer, “Verification of image-based neural network controllers using generative models,” *Journal of Aerospace Information Systems*, 2022.
- [9] M. Mirza and S. Osindero, “Conditional generative adversarial nets,” *arXiv preprint*, 2014.
- [10] K. D. Julian and M. J. Kochenderfer, “Guaranteeing safety for neural network-based aircraft collision avoidance systems,” in *IEEE/AIAA Digital Avionics Systems Conference*, 2019.
- [11] W. Xiang and T. T. Johnson, “Reachability analysis and safety verification for neural network control systems,” *arXiv preprint*, 2018.
- [12] S. Bak, “nnum: Verification of relu neural networks with optimized abstraction refinement,” in *NASA Formal Methods Symposium*, 2021.
- [13] M. Althoff, O. Stursberg, and M. Buss, “Reachability analysis of nonlinear systems with uncertain parameters using conservative linearization,” in *IEEE Conference on Decision and Control*, 2008.
- [14] P. S. Duggirala and M. Viswanathan, “Parsimonious, simulation based verification of linear systems,” in *International Conference on Computer Aided Verification*, 2016.
- [15] H. Zhang, T.-W. Weng, P.-Y. Chen, C.-J. Hsieh, and L. Daniel, “Efficient neural network robustness certification with general activation functions,” *Advances in neural information processing systems*, 2018.
- [16] T. C. Staudinger, Z. D. Jorgensen, and D. D. Margineantu, “X-taxinet-an environment for learning and decision systems for airplane operations,” 2018.
- [17] F. Cai and X. Koutsoukos, “Real-time out-of-distribution detection in learning-enabled cyber-physical systems,” in *ACM/IEEE International Conference on Cyber-Physical Systems*, 2020.
- [18] A. Dosovitskiy, G. Ros, F. Codevilla, A. Lopez, and V. Koltun, “CARLA: An open urban driving simulator,” in *Annual Conference on Robot Learning*, 2017.
- [19] D. M. Lopez, M. Althoff, M. Forets, T. T. Johnson, T. Ladner, and C. Schilling, “Arch-comp23 category report: Artificial intelligence and neural network control systems (aincs) for continuous and hybrid systems plants,” *EPiC Series in Computing*, 2023.
- [20] M. Althoff, “An introduction to cora 2015,” in *Proc. of the 1st and 2nd Workshop on Applied Verification for Continuous and Hybrid Systems*, 2015, pp. 120–151.
- [21] S. Bogomolov, M. Forets, G. Frehse, K. Potomkin, and C. Schilling, “Juliareach: a toolbox for set-based reachability,” in *ACM International Conference on Hybrid Systems: Computation and Control*, 2019.
- [22] J. K. Scott, D. M. Raimondo, G. R. Marsaglia, and R. D. Braatz, “Constrained zonotopes: A new tool for set-based estimation and fault detection,” *Automatica*, vol. 69, pp. 126–136, 2016.
- [23] M. Wetzlinger, N. Kochdumper, S. Bak, and M. Althoff, “Fully automated verification of linear systems using inner-and outer-approximations of reachable sets,” *IEEE Transactions on Automatic Control*, 2023.
- [24] L. Jaulin, M. Kieffer, O. Didrit, E. Walter, L. Jaulin, M. Kieffer, O. Didrit, and É. Walter, *Interval analysis*. Springer, 2001.

- [25] H.-D. Tran, F. Cai, M. L. Diego, P. Musau, T. T. Johnson, and X. Koutsoukos, "Safety verification of cyber-physical systems with reinforcement learning control," *ACM Transactions on Embedded Computing Systems*, 2019.
- [26] H. Zhang, I. Goodfellow, D. Metaxas, and A. Odena, "Self-attention generative adversarial networks," in *International conference on machine learning*, 2019.
- [27] L. Hou, Q. Cao, H. Shen, S. Pan, X. Li, and X. Cheng, "Conditional gans with auxiliary discriminative classifier," in *International Conference on Machine Learning*, 2022.
- [28] M. Kang, W. Shim, M. Cho, and J. Park, "Rebooting acgan: Auxiliary classifier gans with stable training," *Advances in neural information processing systems*, 2021.
- [29] X. Ding, Y. Wang, Z. Xu, W. J. Welch, and Z. J. Wang, "CcGAN: Continuous conditional generative adversarial networks for image generation," in *International Conference on Learning Representations*, 2021.
- [30] S. Tulyakov, M.-Y. Liu, X. Yang, and J. Kautz, "Mocogan: Decomposing motion and content for video generation," in *IEEE conference on computer vision and pattern recognition*, 2018, pp. 1526–1535.